

1 **Seasonal enhancement in upper atmospheric D/H at**
2 **Mars driven by both thermospheric temperature and**
3 **mesospheric water**

4 **E. M. Cangi¹, M. S. Chaffin¹, R. V. Yelle², B. S. Gregory¹, J. Deighan¹**

5 ¹Laboratory for Atmospheric and Space Physics, University of Colorado Boulder

6 ²Lunar and Planetary Laboratory, University of Arizona

7 **Key Points:**

- 8 • Seasonal increases in exobase temperature or mesospheric water can enhance the
9 upper atmospheric atomic D/H ratio up to 25 times VSMOW.
- 10 • The enhancement occurs due to dynamical differences, leading to similarities in
11 D/H ratio but differences in abundance and escape.
- 12 • Concurrent measurements of temperatures, water vapor, and the D/H ratio will
13 enhance our understanding of atmospheric escape from Mars.

Abstract

The D/H ratio in water on Mars, R_{water} , is 4–6× the Earth ratio, signifying past water loss to space. Recently, measurements have revealed high values of the D/H ratio in hydrogen, R_{atomic} , in the thermosphere during southern summer. Here, we use a photochemical model to explore the potential drivers of R_{atomic} , testing three: thermospheric temperatures, excess mesospheric water, and changing insolation. We find that R_{atomic} can achieve values between 15× the Earth ratio (due to water) and 25× the Earth ratio (due to temperature). The effects arise because H escape is diffusion-limited, while D escape is energy-limited. Our results underscore how R_{atomic} reflects mesospheric dynamics, and the need for concurrent measurements of mesospheric water, thermospheric temperatures, and R_{atomic} to understand seasonal changes in the martian water cycle and atmospheric loss.

Plain Language Summary

The high ratio of deuterium (D) to hydrogen (H) measured in water molecules on Mars indicates that much of Mars’ past water has escaped to space. Recent measurements of the D/H ratio in the atoms themselves using data from the MAVEN spacecraft have revealed a ratio as high as 100 times the Earth value. In this work, we use a computational model of the Mars atmosphere to explore whether the large values could be caused by seasonal changes in three atmospheric parameters: the upper atmospheric temperature, the presence of extra water vapor in the middle atmosphere, and the incoming solar radiation. We find that temperature and water vapor have comparable effects, with each leading to an atomic D/H ratio similar to those found by MAVEN observations. We also explain how temperature and water affect the dynamics of H and D in the atmosphere to cause the change in the ratio.

1 Background and Motivation

Isotope ratios in planetary atmospheres encode a history of atmospheric escape. On Mars, the argon isotope system reveals how sputtering has affected atmospheric loss (Jakosky et al., 2017; Slipski & Jakosky, 2016); nitrogen is used to reconstruct potential past atmospheric compositions (e.g. Pieris & Jakosky, 2022; Hu & Thomas, 2022); and hydrogen probes long-term water loss (Owen et al., 1988; Yung et al., 1988; Carr,

1990, and many others). Because of the interest in water loss from Mars, the isotopic ratio of deuterium (D) and hydrogen (H) is typically measured in water as:

$$R_{\text{water}} = \frac{[\text{HDO}]}{2[\text{H}_2\text{O}]}, \quad (1)$$

where square brackets represents a number density (abundance). R_{water} is $4\text{--}6 \times \text{VSMOW}$ (Vienna Standard Mean Ocean Water, the ratio measured in Earth’s oceans) (Owen et al., 1988; Bjoraker et al., 1989; Krasnopolsky et al., 1997; Encrenaz et al., 2018), with local variations between $1\text{--}10 \times \text{VSMOW}$ (Villanueva et al., 2015, 2021, 2022). This enhancement relative to Earth is thought to be driven by escape to space of H and D, which on Mars are primarily sourced from the water molecules H_2O and its isotope HDO.

Despite the key role of the atomic species in the parching of the planet, few measurements exist of the atomic D/H ratio,

$$R_{\text{atomic}} = \frac{[\text{D}]}{[\text{H}]}. \quad (2)$$

This is mainly due to measurement difficulties: a high resolution is required to resolve the H and D Lyman α emissions. Some measurements have been made using the Hubble Space Telescope’s Goddard High Resolution Spectrograph and Space Telescope Imaging Spectrograph (Bertaux et al., 1992; Krasnopolsky et al., 1998; Clarke et al., 2006) during Mars aphelion. Combined with these, new results obtained with the MAVEN (Mars Atmosphere and Volatile Evolution) IUVS (Imaging UltraViolet Spectrograph) throughout the Mars year suggest a strong seasonal variation in H and D brightness and the derived R_{atomic} (Clarke et al., 2022; Chaufray et al., 2021), distinct from effects of individual dust storms, suggesting a repeatable, seasonal driver. Because the emission brightness of Lyman α directly probes the escaping atomic species, these measurements enable additional insight into atmospheric escape.

In this work, we study the sub-annual response of R_{atomic} due to seasonal perturbations and the driving dynamical or chemical processes. We use a 1D photochemical model (E. M. Cangi et al., 2023) to explore three options for the driver of R_{atomic} enhancements: greater thermospheric temperatures, which have a significant effect on the D/H fractionation factor (E. M. Cangi et al., 2020); changing insolation, which affects

70 photodissociation and ionization and atmospheric chemistry; or increased mesospheric
 71 water, demonstrated to enhance H escape (e.g. Chaffin et al., 2021; Stone et al., 2020;
 72 Chaffin et al., 2017). To simulate an annual cycle and examine the time-dependent pho-
 73 tochemistry of the atmosphere, we simulate one Mars season per model run, using the
 74 output of one run as input for the next. We find that the thermospheric temperature
 75 and mesospheric water can both cause significant variations in R_{atomic} , while insolation
 76 changes are negligible.

77 Our present work demonstrates how subtle differences in the underlying dynam-
 78 ics of H and D lead to similarities in their thermospheric ratio, but differences in their
 79 abundances in the upper atmosphere and escape to space. This suggests the possibil-
 80 ity of using measurements of D/H in atoms in the thermosphere as a probe for meso-
 81 spheric dynamics. We thus highlight a need for concurrent observations of D/H, ther-
 82 mal structure, and atmospheric water abundances from surface to space to enable new
 83 insights into atmospheric escape and water loss from Mars.

84 2 Modeling methods

85 We use the same modeling approach as E. M. Cangi et al. (2023). Full details of
 86 the model, bluejay, are available in that paper and the archived code (E. Cangi & Chaf-
 87 fin, 2023), and the model parameters are summarized in Table S1. The three variable
 88 atmospheric parameters of thermospheric temperature, mesospheric water, and solar in-
 89 put are handled by the model in the following ways:

- 90 1. **Thermospheric temperature:** Past work has shown that the thermospheric tem-
 91 perature strongly affects D/H fractionation (E. M. Cangi et al., 2020) and Jeans
 92 escape. Our model prescribes temperature as a function of altitude, controlling
 93 it by modifying T_{exo} , the temperature at top of the model (250 km). T_{exo} can take
 94 on the values 175 K (“winter”-like conditions), 225 K (“spring”/“fall”), or 275 K
 95 (“summer”).
- 96 2. **Mesospheric water abundance:** Water can enter the mesosphere due to dust
 97 activity (Villanueva et al., 2021; Chaffin et al., 2021; Holmes et al., 2021; Stone
 98 et al., 2020; A. A. Fedorova et al., 2020; Vandaele et al., 2019; Aoki et al., 2019;
 99 Heavens et al., 2018; Chaffin et al., 2021) or other seasonal effects (Shaposhnikov
 100 et al., 2019; Neary et al., 2020), driving H escape (Chaffin et al., 2021; Stone et

101 al., 2020). In our model, we prescribe water abundance below 72 km, allowing the
 102 model to solve for the abundance above that level. We define three scenarios: a
 103 dry mesosphere (“aphelion” conditions), a mesosphere with average moisture, and
 104 a wet mesosphere (“perihelion”).

105 **3. Insolation:** Mars’ orbit is eccentric, which affects the amount of UV insolation
 106 available to drive photodissociation and ionization of atmospheric molecules. We
 107 use the solar spectra for at 1.67 AU, 1.524 AU, and 1.38 AU.

108 As mentioned, the effect of the insolation variation was negligible (see Figure S2),
 109 and will not be discussed. We also explored a set with extra water added in the lower
 110 atmosphere (see Figure S7), but this also had a negligible effect on R_{atomic} .

111 Timesteps in the model are logarithmic; they start small ($dt \approx 10^{-3}$ seconds) and
 112 become larger near the end ($dt \approx 10^7$ seconds). The model state is saved in quasi-logarithmically
 113 spaced points from 1 second to 1 day, then once per week after. This scheme is shown
 114 in Figure S1.

115 We use the best available photodissociation cross sections for HDO (Cheng et al.,
 116 1999, 2004; Chung et al., 2001). We also ran several simulations in which both H_2O and
 117 HDO use the H_2O cross sections, resulting in a $2.5\times$ larger ratio around 60 km, consis-
 118 tent with Alday et al. (2021), but a negligible change to the D/H ratio above 80 km (see
 119 Figures S4 and S10).

120 We run three sets of simulations: “Temperature”, “Water”, and “Insolation”. For
 121 each set, we model an annual cycle by imposing the appropriate seasonal input param-
 122 eters on the model, running it for one “season” (1/4 of a Mars year, $\sim 1.48 \times 10^7$ sec-
 123 onds), and then using the atmospheric state at the end of each simulation as the initial
 124 conditions for the next season in the cycle. In all simulations, there are no sub-seasonal
 125 changes in the temperature profile, the water profile below 72 km, or the insolation pro-
 126 file, in order to clearly separate the atmospheric response to a forcing impulse.

127 **3 Two controls on escape to space: energy and supply**

128 Two major variables affect the escape of light atoms like H and D to space: the amount
 129 of energy available to these atoms, and their total abundance in the upper atmosphere.

130 In order to escape from the atmosphere, atoms must do two things: reach the escape re-
 131 gion (exobase), and gain enough energy to exceed escape velocity.

132 The importance of energy is fairly straightforward. Atoms with velocities in the
 133 high-energy tail of the Maxwell-Boltzmann distribution have enough energy to escape
 134 in the thermal Jeans escape regime; other atoms do not, but may gain excess energy through
 135 non-thermal processes, mostly involving ions or the solar wind in some way (Hunten, 1982).
 136 Previous work has shown that the mass difference of H and D leads to H escape being
 137 mostly thermal, while D escape is mostly non-thermal (E. M. Cangi et al., 2023; Krasnopol-
 138 sky, 2002).

Supply is slightly more complex, and requires us to consider the atmosphere as an
 integrated whole. Water is the main reservoir of H and D at Mars, and is primarily present
 in the lower atmosphere. This means that the lower atmosphere is a source region for
 H and D, which are freed when water dissociates and then transport up toward the exobase.
 As temperatures rise and the atmosphere expands, the density of heavier species at a
 given altitude near the homopause increases, making it more difficult for H and D to dif-
 fuse upward due to more frequent collisions (Mayyasi et al., 2018), thus limiting the sup-
 ply of atoms to the thermosphere. There is thus some maximum vertical flux of light gases.
 The limiting flux (Hunten, 1973) has been used to describe the maximum upward flux
 of a species possible in an isothermal atmosphere, defined as follows (Hunten, 1973):

$$\phi_\ell \approx \frac{D_i n_i}{H_a} \left(1 - \frac{m_i}{m_a} \right) \quad (3)$$

$$\approx \frac{b f_i}{H_a} \quad (\text{for minor species}), \quad (4)$$

139 where D_i , n_i and m_i are the diffusion coefficient, density, and mass of species i , and H_a
 140 and m_a are the mean scale height and molecular mass of the background atmosphere.
 141 Equation 4 is valid for minor species like H and D; here b is the binary diffusion param-
 142 eter, and f_i is the mixing ratio of species i . When the actual vertical flux of a species
 143 equals the limiting flux, $\phi_{\text{esc}} = \phi_\ell$, the mixing ratio of that species is constant with height
 144 and its escape to space is described as diffusion-limited (Hunten, 1973).

145 The limiting flux does not apply perfectly throughout real atmospheres, which are
 146 typically not isothermal and have complex chemistry and transport. In studies of Mars,
 147 the limiting flux is typically evaluated at the homopause, near the top of the mesosphere,

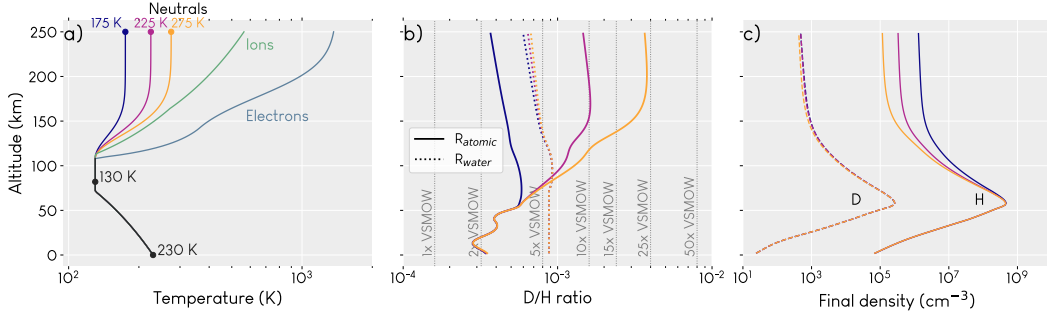


Figure 1. a) Model input: Temperature profiles adopted to simulate seasonal variation. b) Model output: Response of the D/H atmospheric profile (at the end of the associated simulation)/season. c) Associated D & H density profiles. Note that in panels b and c, the colors of the lines map to the neutral temperatures in panel a.

148 which separates the lower atmospheric source of H and D and the escape region (e.g. Zahnle
 149 et al., 2008). The mesosphere is also the only part of the atmosphere that is at all close
 150 to isothermal. Using our model, we can calculate representative limiting fluxes using equa-
 151 tion 4 and compare to typical escape values. For H, $\phi_{\text{esc,H}} = 1-1.1 \times 10^8 \text{ cm}^{-2}\text{s}^{-1}$ (Jakosky
 152 et al., 2018), but the representative limiting flux is $\phi_{\ell,H} = 4-6 \times 10^8 \text{ cm}^{-2}\text{s}^{-1}$. The
 153 similarity in $\phi_{\ell,H}$ and $\phi_{\text{esc,H}}$ means that supply to the upper atmosphere is the most sig-
 154 nificant barrier to H escape. On the other hand, for D, the typical escape rate is $\phi_{\text{esc,D}} =$
 155 $5-14 \times 10^3 \text{ cm}^{-2}\text{s}^{-1}$ (E. M. Cangi et al., 2023), and the representative limiting flux is
 156 $\phi_{\ell,D} = 4-5 \times 10^5 \text{ cm}^{-2}\text{s}^{-1}$. The limiting flux being larger than the escape flux means
 157 that upper atmospheric supply is not a barrier to escape for D; rather, due to D’s higher
 158 mass, its energy is the more important controlling factor of its escape. Essentially, on
 159 Mars, H escape is diffusion-limited (or supply-limited), while D escape is energy-limited
 160 (sometimes also called kinetically limited).

161 For the remainder of this paper, we will discuss energy-limited escape mostly in
 162 reference to D, and diffusion-limited escape in reference to H.

163 4 Warmer exospheric temperatures increase R_{atomic} by driving H es- 164 cape and throttling resupply from below

165 Figures 1 and 2 show the model results from variation of the exobase temperature
 166 (which also changes the overall thermospheric temperature, due to the functional form
 167 we use for temperature), with altitude profiles of R_{atomic} and H and D densities shown

168 in Figure 1 and time evolution of R_{atomic} , the densities, and their escape fluxes shown
 169 in Figure 2.

170 Figure 1a shows the temperature profiles adopted. Ion and electron profiles are held
 171 fixed due to limited new data available to constrain them (E. M. Cangi et al., 2023; Han-
 172 ley et al., 2022) and the fact that due to observing geometries and instrument pointing
 173 requirements, it is difficult to obtain simultaneous temperature measurements of differ-
 174 ent populations such as neutrals and ions (Gupta et al., 2022). Panel 1b shows how R_{atomic}
 175 and R_{water} respond; R_{water} is mostly unaffected, while R_{atomic} ranges from 2 to nearly
 176 $25\times$ VSMOW in the upper atmosphere. This response is largest in the atoms; D/H ra-
 177 tios in other species are less pronounced (see Figure S3). Figure 1c shows a minimal change
 178 to upper atmospheric D, whereas a higher temperature leads to a $10\times$ rarefaction of H,
 179 the same amount by which the D/H ratio increases.

180 Figure 2 shows the same information over the full annual cycle by placing time on
 181 the horizontal axis. Panel 2c shows even more clearly that the primary driver of the in-
 182 crease in R_{atomic} is the large decrease of the H density.

183 The responses of D and H escape to temperature perturbations are dissimilar, as
 184 shown in panels 2d and e. As explained previously, H escape is diffusion-limited, and es-
 185 cape depends on both energy available to the escaping atoms and supply of said atoms.
 186 Thus, when the temperature rises, a larger fraction of upper atmospheric H suddenly has
 187 enough energy to escape, creating the spikes in flux in panel 2d. However, the resupply
 188 of H from below is mostly unchanged, so after a short time, the thermospheric H den-
 189 sity decreases and H escape returns to its prior value, but the density of H at the exobase
 190 is depleted (as discussed by Mayyasi et al., 2018). A similar effect occurs when the tem-
 191 perature drops: less energy available means the escape rate suddenly drops, allowing the
 192 H abundance near the exobase to rebound, later returning the escape rate to its prior
 193 value. The net effect to the seasonally-integrated escape rate is negligible.

194 On the other hand, as long as the temperature is enhanced, so too is D escape, which
 195 is energy-limited. There was already plenty of D in the escape region that only needed
 196 some extra energy (which is made available by the temperature increase) to escape.

197 The uniqueness of H as a diffusion-limited species on Mars is important in under-
 198 standing D/H variations and escape; the D/H ratio of other isotopologue pairs (see Fig-

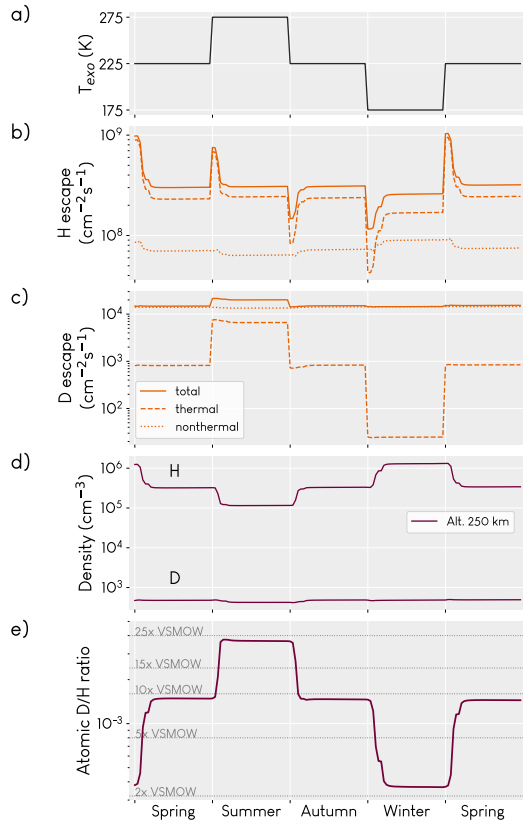


Figure 2. Atmospheric behavior over one Mars year. a) Model input: Exobase temperature. b) H and c) D escape to space (total, thermal, and non-thermal) in response to the temperature changes of panel a). d) Changes to H and D densities as a result of escape and vertical transport. e) The resulting effects on R_{atomic} .

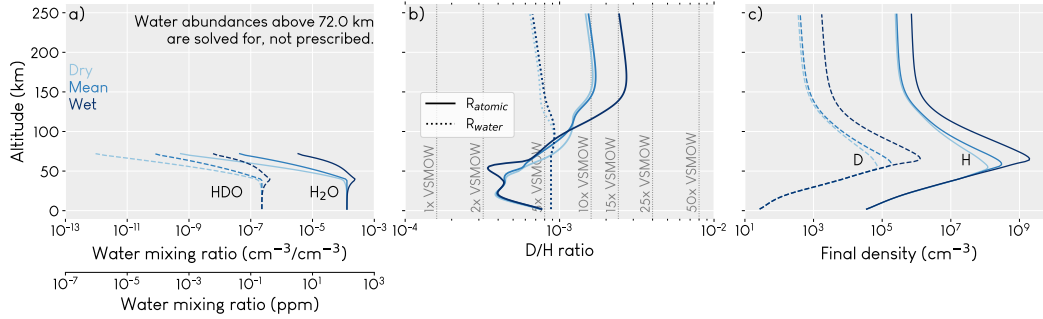


Figure 3. The same as Figure 1, but for different initial mesospheric water abundances (panel a). In panel a, which shows the initial state, we do not include the upper atmosphere (which is solved for in the model). The profile with the most water has a peak mixing ratio of nearly 300 ppm of water at its peak, which is comparable to what has been observed during dust storms (e.g. Vandaele et al., 2019).

199 ure S3) do not show such dramatic temperature dependence, as heavier molecules in these
 200 other isotopologue pairs are less abundant and do not escape as readily as H or D.

201 **5 Extra mesospheric water increases R_{atomic} by supplying more H above**
 202 **the mesosphere**

203 Figure 3 shows the altitude profiles of R_{atomic} and D and H densities that result
 204 from varying the mesospheric water abundance. Changing the water abundance in the
 205 mesosphere makes only a small difference in the total amount of water in the atmosphere
 206 (in precipitable micrometers, it is 10.4, 10.5, and 10.9 pr μm for the low, mean, and high
 207 water cases respectively).

208 Our “perihelion” water profile has nearly 300 ppm at its peak in the mesosphere,
 209 which is similar to observations during dust storms, (e.g. Vandaele et al., 2019) and was
 210 chosen to demonstrate an edge case of high water conditions. Perturbations of this mag-
 211 nitude to the water profile can also spur an enhancement of R_{atomic} (Figure 3b), but with
 212 a smaller magnitude (to 10-15 \times VSMOW, compared with 2-25 \times VSMOW in Figure 2c).
 213 Figure S8 also shows the D/H ratio in other species.

214 When water is introduced into the mesosphere, D and H respond differently. The
 215 abundances of both species peak at a higher altitude as mesospheric water increases, which
 216 is logical given the greater abundance of source water molecules at higher altitudes. The

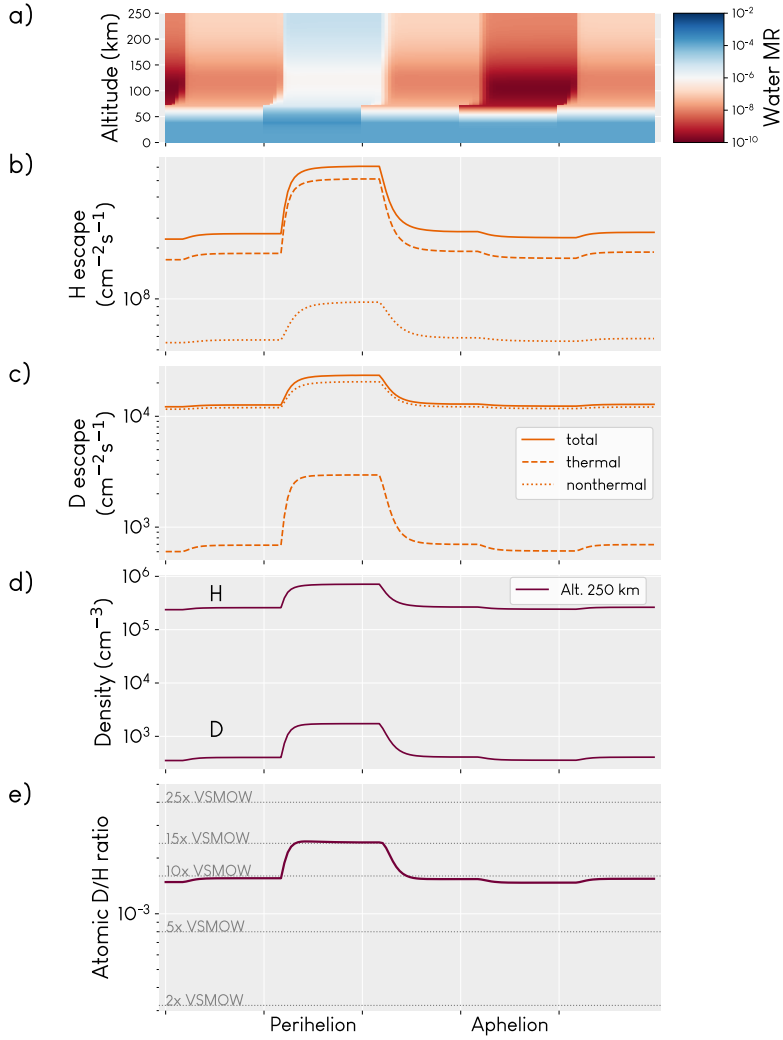


Figure 4. The same as Figure 2, but in response to changing water abundance in the mesosphere, which also propagates upwards. Because the water is supplied above the cold trap, both H and D escape in this scenario are sustained throughout the perihelion season, and the D/H ratio also increases because H escape increases relatively more than D escape.

217 increase in upper atmospheric D density also exhibits a stronger response to the pertur-
 218 bation than H. This is because no additional energy has come into the system, only sup-
 219 ply; thus, D escape does increase somewhat, but not as much as H escape.

220 The relative changes in escape and density of H and D as a result of mesospheric
 221 water are shown in Figure 4. Adding water into the mesosphere has two main effects.
 222 First, the dissociated water supplies both D and H to the upper atmosphere. This ad-
 223 ditional supply enables a greater enhancement of H escape (150% increase) than D es-

224 cape (85% increase). This is because diffusion-limited H escape is most strongly controlled
 225 by the supply of escape-capable atoms, while the main control on D escape is the energy
 226 available. We have not changed the temperature (and therefore the energy) in this sce-
 227 nario, so the overall change to D escape is smaller than for H escape. Second, this pref-
 228 erential enhancement of H escape means that the increase of H (a 145% increase) in the
 229 upper atmosphere is less pronounced than for D (a 282% increase).

230 Because of the greater relative enhancement of H escape, we should also expect to
 231 see a decreased fractionation factor of escape (E. M. Cangi et al., 2020) when the meso-
 232 sphere has extra water; this expectation is confirmed in Figure S9.

233 6 Discussion

234 The key takeaway is: both thermospheric temperature variations and mesospheric
 235 water abundance variations can affect the value of R_{atomic} in the upper atmosphere with
 236 similar efficacy, but differ in the effects on escape and raw abundance.

237 Seasonal periods of high thermospheric temperatures increase R_{atomic} by deplet-
 238 ing the upper atmosphere of H. This depletion occurs due to a brief enhancement of H
 239 escape (Figure 2d) and reduced, diffusion-limited re-supply from below. At the same time,
 240 D escape is enhanced slightly, but not enough to meaningfully deplete the upper atmo-
 241 sphere of D (Figures 1 and 2), and the elevated, energy-limited escape can be sustained
 242 as long as the temperature perturbation lasts (Figure 2e). A similar effect on H has been
 243 observed during space weather events with MAVEN. In September 2017, heightened so-
 244 lar activity briefly enhanced thermospheric heating caused a 25% decrease in H density
 245 and a temporary $5\times$ increase in H escape (Mayyasi et al., 2018), comparable to seasonal
 246 variations in H escape.

247 Seasonal mesospheric water releases extra H and D atoms, increasing the supply
 248 of atoms that can more easily reach the escape region. This means that escape of both
 249 H and D is sustained while the water perturbation is present. Because of the diffusion-
 250 limited nature of H escape, a relatively greater proportion of the H supplied to the up-
 251 per atmosphere will escape compared to the supplied D. This leads to a build-up of D
 252 in the upper atmosphere and an enhanced R_{atomic} .

253 Close examination of Figure 4 will reveal that while thermal H escape increases by
 254 a factor of $\sim 2.5\times$ after the introduction of mesospheric water, non-thermal escape only

255 increases by a factor of ~ 2 . This is likely because the dissociation of water leads directly
256 to the creation of neutral H (D), which can then escape thermally. On the other hand,
257 non-thermal escape occurs when hot H (D) is created in ionospheric reactions, most im-
258 portantly HCO^+ (DCO^+) dissociative recombination (E. M. Cangi et al., 2023; Gregory
259 et al., 2023). HCO^+ (DCO^+) is a terminal ion (Fox, 2015), so neutral H (D) in the up-
260 per atmosphere must first be incorporated into HCO^+ (DCO^+) and then later be freed
261 through dissociative recombination before it can escape non-thermally; evidently, these
262 chemical pathways are already saturated. Along the way, neutral H (D) may also find
263 its way into a number of other species; in essence, the path for H (D) to non-thermal es-
264 cape is less direct than to thermal escape.

265 Not all atoms escape. Some H and D may also mix downwards, which is required
266 for the exchangeable reservoir of water to attain its present D/H ratio. It is difficult to
267 quantify the exact amounts which mix down, as we do not track individual atoms, but
268 we can estimate the amount of escape relative to the total H and D columns. Figures
269 S5 and S11 show the same information as Figures 2 and 4, but with an additional plot-
270 ted line showing the fraction of the total H or D column which escapes; for H, this is \sim
271 $4 \times 10^{-5}\%$ (0.4 ppm) on average, and for D, $\sim 3 \times 10^{-6}\%$ (0.03 ppm, 30 ppb). The
272 D/H ratio of escaping atoms is also rarely higher than $1 \times$ VSMOW (see Figures S6 and
273 S12), consistent with the notion that even in periods of elevated D escape, most D is re-
274 tained on the planet.

275 Apart from the drivers of R_{atomic} discussed here, other fractionating processes may
276 add nuance to the mobilization or retention of D. One is the preferential condensation
277 of HDO over H_2O (Bertaux & Montmessin, 2001; Lamb et al., 2017), which may tem-
278 porarily reduce D escape by sequestering it in the seasonal water ice polar caps (Fisher,
279 2007; Vos et al., 2022) and clouds (Moores, Osinski, et al., 2011). On the other hand,
280 adsorption fractionation of water on dust grains has a fractionation factor of 1.97 ± 0.74 ,
281 leading to a D/H ratio up to $21 \times$ VSMOW in adsorbed water (Moores, Smith, & Boynton,
282 2011). Little dust has been observed above 60 km, so dust adsorption/desorption
283 is not thought to be a direct delivery method for water above that altitude (Neary et
284 al., 2020; Vandaele et al., 2019; A. Fedorova et al., 2018), but the process may enable
285 D to reach the bottom of the mesosphere; at present, dedicated studies in this area are
286 not available in the literature.

287 Similarly large values of R_{atomic} have been observed at Mars with the MAVEN IUVS
 288 instrument. Using the low resolution mode, Chaufray et al. (2021) calculated R_{atomic} at
 289 200 km and $T = 220$ K up to $1.7 \pm 0.4 \times 10^{-2}$, or $106 \times$ VSMOW; other values range
 290 as low as $1 \times$ VSMOW, but frequently fall between $20\text{--}40 \times$ VSMOW. Through obser-
 291 vations of the H corona, Chaffin et al. (2018) calculated $R_{\text{atomic}} = 20\text{--}91 \times$ VSMOW. Mea-
 292 surements of R_{atomic} using the echelle channel (higher resolution) are also currently un-
 293 derway, with initial results hinting at a strong seasonal response in both D and H bright-
 294 ness and R_{atomic} (Clarke et al., 2022). Past work by the same team has also revealed sea-
 295 sonal enhancement of atomic D brightness without a concurrent atomic D/H ratio cal-
 296 culation (Mayyasi et al., 2019). Our results generally agree with these measurements while
 297 also adding the important context of the two distinct drivers of R_{atomic} .

298 7 Conclusion

299 Our results demonstrate that thermospheric R_{atomic} , rather than R_{water} , is more
 300 sensitive to short-term perturbations in the atmospheric system due to its sensitive de-
 301 pendence on both thermospheric temperature and mesospheric water. Seasonal changes
 302 to these two parameters lead to similar effects on R_{atomic} , but affect the thermospheric
 303 abundances of D and H and their escape rates differently. The cause of these variations
 304 in the thermosphere is differences in the dynamics of H and D in the mesosphere; H es-
 305 cape is diffusion-limited, while D escape is energy-limited.

306 Mars is unique in the fact that its gravity, atmospheric pressure and thickness, and
 307 presence of water vapor combine to create a situation where the diffusion and escape be-
 308 haviors of H and D are so different. Since other planets in the solar system have either
 309 much higher gravity, thicker atmospheres, or much less water, the same situation may
 310 not arise for H and D on other bodies. However, the lessons learned here may be poten-
 311 tially applied to other isotope systems on other terrestrial planets with atmospheres.

312 Cross-correlation of martian datasets containing upper atmospheric R_{atomic} , ther-
 313 mospheric temperatures, and mesospheric water would enhance our understanding of the
 314 martian climate and water cycle. Concurrent measurements could be ingested into pho-
 315 tochemical and climate models, providing realistic constraints, refining estimates of at-
 316 mospheric escape, and helping to identify knowledge gaps. Such an approach could also

317 provide insight into the dynamics of water, H, and D in the relatively difficult-to-observe
 318 upper mesosphere and lower thermosphere ($\sim 80\text{-}110$ km).

319 In our quest to understand the long-term evolution of the stability of water on ter-
 320 restrial planets, we must continue working both to understand the specific effects of in-
 321 dividual processes and to develop synoptic-scale understanding of the complex ways that
 322 surfaces and atmospheres interact and alter one another.

323 8 Open Research

324 Our model, bluejay, is available on Zenodo (E. Cangi & Chaffin, 2023); the work-
 325 ing copy is available in the linked Github repository. bluejay is written for Julia 1.8.5
 326 (Bezanson et al., 2017).

327 Acknowledgments

328 This work was supported by three primary funding sources. First, this material is based
 329 upon work supported by the National Science Foundation Graduate Research Fellow-
 330 ship Program under Grant DGE 1650115. Any opinions, findings, and conclusions or rec-
 331 ommendations expressed in this material are those of the author(s) and do not neces-
 332 sarily reflect the views of the National Science Foundation. Second, this work was sup-
 333 ported by NASA’s FINESST Program (Grant 80NSSC22K1326). Third, this work was
 334 supposed by NASA through the MAVEN project.

335 References

- 336 Alday, J., Trokhimovskiy, A., Irwin, P. G. J., Wilson, C. F., Montmessin, F.,
 337 Lefèvre, F., . . . Shakun, A. (2021, June). Isotopic fractionation of water
 338 and its photolytic products in the atmosphere of Mars. *Nature Astronomy*, *5*,
 339 943-950. doi: 10.1038/s41550-021-01389-x
- 340 Aoki, S., Vandaele, A. C., Daerden, F., Villanueva, G. L., Liuzzi, G., Thomas, I. R.,
 341 . . . Lopez-Moreno, J. J. (2019, December). Water Vapor Vertical Profiles on
 342 Mars in Dust Storms Observed by TGO/NOMAD. *Journal of Geophysical*
 343 *Research (Planets)*, *124*(12), 3482-3497. doi: 10.1029/2019JE006109
- 344 Bertaux, J. L., Clarke, J. T., Mumma, M., Owen, T., & Quemerais, E. (1992,
 345 January). A Search for the Deuterium Lyman-alpha Emission from the Atmo-
 346 sphere of Mars. In *European southern observatory conference and workshop*

- 347 *proceedings* (Vol. 44, p. 459).
- 348 Bertaux, J.-L., & Montmessin, F. (2001, December). Isotopic fractionation through
349 water vapor condensation: The Deuteropause, a cold trap for deuterium in the
350 atmosphere of Mars. , *106*(E12), 32879-32884. doi: 10.1029/2000JE001358
- 351 Bezanson, J., Edelman, A., Karpinski, S., & Shah, V. B. (2017). Julia: A fresh ap-
352 proach to numerical computing. *SIAM review*, *59*(1), 65–98.
- 353 Bjoraker, G. L., Mumma, M., & Larson, H. P. (1989). Isotopic Abundance Ra-
354 tios for Hydrogen and Oxygen in the Martian Atmosphere. In *Bulletin of the*
355 *American Astronomical Society* (Vol. 21, p. 991).
- 356 Cangì, E., & Chaffin, M. (2023, October). *bluejay: atmospheric photochemistry in*
357 *Julia*. Retrieved from <https://doi.org/10.5281/zenodo.8432604>
- 358 Cangì, E. M., Chaffin, M. S., & Deighan, J. (2020). Higher Martian Atmospheric
359 Temperatures at All Altitudes Increase the D/H Fractionation Factor and
360 Water Loss. *Journal of Geophysical Research: Planets*, *125*(12), 1–15. doi:
361 10.1029/2020JE006626
- 362 Cangì, E. M., Chaffin, M. S., Yelle, R. V., Gregory, B. S., & Deighan, J. (2023).
363 Fully coupled photochemistry of the deuterated ionosphere of Mars and its
364 effects on escape of H and D. *Journal of Geophysical Research: Planets*,
365 *tbd*(*tbd*), *tbd*. doi: *tbd*
- 366 Carr, M. H. (1990, September). D/H on Mars: Effects of floods, volcanism, impacts,
367 and polar processes. , *87*(1), 210-227. doi: 10.1016/0019-1035(90)90031-4
- 368 Chaffin, M. S., Chaufray, J. Y., Deighan, J., Schneider, N. M., Mayyasi, M., Clarke,
369 J. T., ... Jakosky, B. M. (2018, August). Mars H Escape Rates Derived From
370 MAVEN/IUVS Lyman Alpha Brightness Measurements and Their Dependence
371 on Model Assumptions. *Journal of Geophysical Research (Planets)*, *123*(8),
372 2192-2210. doi: 10.1029/2018JE005574
- 373 Chaffin, M. S., Deighan, J., Schneider, N. M., & Stewart, A. I. F. (2017, January).
374 Elevated atmospheric escape of atomic hydrogen from Mars induced by high-
375 altitude water. *Nature Geoscience*, *10*(3), 174-178. doi: 10.1038/ngeo2887
- 376 Chaffin, M. S., Kass, D. M., Aoki, S., Fedorova, A. A., Deighan, J., Connour,
377 K., ... Korablev, O. I. (2021, August). Martian water loss to space en-
378 hanced by regional dust storms. *Nature Astronomy*, *5*, 1036-1042. doi:
379 10.1038/s41550-021-01425-w

- 380 Chaufray, J. Y., Mayyasi, M., Chaffin, M., Deighan, J., Bhattacharyya, D.,
 381 Clarke, J., ... Jakosky, B. (2021, April). Estimate of the D/H Ratio in
 382 the Martian Upper Atmosphere from the Low Spectral Resolution Mode of
 383 MAVEN/IUVS. *Journal of Geophysical Research (Planets)*, 126(4), e06814.
 384 doi: 10.1029/2020JE006814
- 385 Cheng, B. M., Chew, E. P., Liu, C. P., Bahou, M., Lee, Y. P., Yung, Y. L., & Ger-
 386 stell, M. F. (1999). Photo-induced fractionation of water isotopomers in the
 387 Martian atmosphere. *Geophysical Research Letters*, 26(24), 3657–3660. doi:
 388 10.1029/1999GL008367
- 389 Cheng, B. M., Chung, C. Y., Bahou, M., Lee, Y. P., Lee, L. C., Van Harreveld, R., &
 390 Van Hemert, M. C. (2004). Quantitative spectroscopic and theoretical study of
 391 the optical absorption spectra of H₂O, HOD, and D₂O in the 125-145 nm re-
 392 gion. *Journal of Chemical Physics*, 120(1), 224–229. doi: 10.1063/1.1630304
- 393 Chung, C. Y., Chew, E. P., Cheng, B. M., Bahou, M., & Lee, Y. P. (2001). Tem-
 394 perature dependence of absorption cross-section of H₂O, HOD, and D₂O
 395 in the spectral region 140-193nm. *Nuclear Instruments and Methods in*
 396 *Physics Research, Section A: Accelerators, Spectrometers, Detectors and*
 397 *Associated Equipment*, 467-468, 1572–1576. (ISBN: 8863578028) doi:
 398 10.1016/S0168-9002(01)00762-8
- 399 Clarke, J. T., Bertaux, J., Chaufray, J., Owen, T., Nagy, A., & Gladstone, R. (2006,
 400 September). HST/Stis Observations Of The D/H Ratio In The Martian Up-
 401 per Atmosphere. In *Aas/division for planetary sciences meeting abstracts #38*
 402 (Vol. 38, p. 60.13).
- 403 Clarke, J. T., Mayyasi, M., Bhattacharyya, D., & Chaufray, J. Y. (2022, June).
 404 Observations of H and D Densities and Escape Fluxes from the Upper At-
 405 mosphere of Mars with the MAVEN IUVS Echelle Channel. In *Seventh in-*
 406 *ternational workshop on the mars atmosphere: Modelling and observations*
 407 (p. 3101).
- 408 Encrenaz, T., DeWitt, C., Richter, M. J., Greathouse, T. K., Fouchet, T.,
 409 Montmessin, F., ... Sagawa, H. (2018, April). New measurements of D/H
 410 on Mars using EXES aboard SOFIA. , 612, A112. doi: 10.1051/0004-6361/
 411 201732367
- 412 Fedorova, A., Bertaux, J.-L., Betsis, D., Montmessin, F., Korabiev, O., Malt-

- 413 agliati, L., & Clarke, J. (2018, January). Water vapor in the middle at-
 414 mosphere of Mars during the 2007 global dust storm. , *300*, 440-457. doi:
 415 10.1016/j.icarus.2017.09.025
- 416 Fedorova, A. A., Montmessin, F., Korablev, O., Luginin, M., Trokhimovskiy, A.,
 417 Belyaev, D. A., . . . Wilson, C. F. (2020, January). Stormy water on Mars:
 418 The distribution and saturation of atmospheric water during the dusty season.
 419 *Science*, *367*(6475), 297-300. doi: 10.1126/science.aay9522
- 420 Fisher, D. A. (2007, April). Mars' water isotope (D/H) history in the strata of the
 421 North Polar Cap: Inferences about the water cycle. , *187*(2), 430-441. doi: 10
 422 .1016/j.icarus.2006.10.032
- 423 Fox, J. L. (2015, May). The chemistry of protonated species in the martian iono-
 424 sphere. *Icarus*, *252*, 366-392. doi: 10.1016/j.icarus.2015.01.010
- 425 Gregory, B. S., Chaffin, M. S., Elliott, R. D., Deighan, J., Gröller, H., & Cangi,
 426 E. M. (2023). Quantifying hot hydrogen escape at Mars via multiple pho-
 427 tochemical mechanisms. *Journal of Geophysical Research: Planets*, (to be
 428 submitted).
- 429 Gupta, S., Yelle, R. V., Schneider, N. M., Jain, S. K., González-Galindo, F., Verdier,
 430 L., . . . Curry, S. (2022, November). Thermal Structure of the Martian Upper
 431 Mesosphere/Lower Thermosphere From MAVEN/IUVS Stellar Occultations.
 432 *Journal of Geophysical Research (Planets)*, *127*(11), e2022JE007534. doi:
 433 10.1029/2022JE007534
- 434 Hanley, K. G., Fowler, C. M., McFadden, J. P., Mitchell, D. L., & Curry, S. (2022,
 435 September). MAVEN-STATIC Observations of Ion Temperature and Ini-
 436 tial Ion Acceleration in the Martian Ionosphere. , *49*(18), e00182. doi:
 437 10.1029/2022GL100182
- 438 Heavens, N. G., Kleinböhl, A., Chaffin, M. S., et al. (2018). Hydrogen escape from
 439 Mars enhanced by deep convection in dust storms. *Nature Astronomy*, *2*. doi:
 440 10.1038/s41550-017-0353-4
- 441 Holmes, J. A., Lewis, S. R., Patel, M. R., Chaffin, M. S., Cangi, E. M., Deighan,
 442 J., . . . Vandaale, A. C. (2021, October). Enhanced water loss from the
 443 martian atmosphere during a regional-scale dust storm and implications for
 444 long-term water loss. *Earth and Planetary Science Letters*, *571*, 117109. doi:
 445 10.1016/j.epsl.2021.117109

- 446 Hu, R., & Thomas, T. B. (2022, February). A nitrogen-rich atmosphere on ancient
447 Mars consistent with isotopic evolution models. *Nature Geoscience*, *15*(2), 106-
448 111. doi: 10.1038/s41561-021-00886-y
- 449 Hunten, D. M. (1973). The escape of light gases from planetary atmospheres. *Jour-
450 nal of Atmospheric Sciences*, *30*(8), 1481–1494.
- 451 Hunten, D. M. (1982, August). Thermal and nonthermal escape mechanisms for ter-
452 restrial bodies. *Planetary and Space Science*, *30*(8), 773-783. doi: 10.1016/
453 0032-0633(82)90110-6
- 454 Jakosky, B. M., Brain, D., Chaffin, M., Curry, S., Deighan, J., Grebowsky, J., ...
455 Zurek, R. (2018, November). Loss of the Martian atmosphere to space:
456 Present-day loss rates determined from MAVEN observations and integrated
457 loss through time. , *315*, 146-157. doi: 10.1016/j.icarus.2018.05.030
- 458 Jakosky, B. M., Slipski, M., Benna, M., Mahaffy, P., Elrod, M., Yelle, R., ... Al-
459 saeed, N. (2017, March). Mars' atmospheric history derived from upper-
460 atmosphere measurements of $^{38}\text{Ar}/^{36}\text{Ar}$. *Science*, *355*(6332), 1408-1410. doi:
461 10.1126/science.aai7721
- 462 Krasnopolsky, V., Bjoraker, G., Mumma, M., & Jennings, D. (1997). High-resolution
463 spectroscopy of Mars at 3.7 and 8 μm : A sensitive search for H_2O_2 , H_2CO ,
464 HCl , and CH_4 , and detection of HDO . *Journal of Geophysical Research*, *102*.
465 doi: 10.1029/96JE03766
- 466 Krasnopolsky, V. A. (2002, December). Mars' upper atmosphere and iono-
467 sphere at low, medium, and high solar activities: Implications for evolution
468 of water. *Journal of Geophysical Research (Planets)*, *107*(E12), 5128. doi:
469 10.1029/2001JE001809
- 470 Krasnopolsky, V. A., Mumma, M. J., & Randall Gladstone, G. (1998, June). De-
471 tection of Atomic Deuterium in the Upper Atmosphere of Mars. *Science*, *280*,
472 1576. doi: 10.1126/science.280.5369.1576
- 473 Lamb, K. D., Clouser, B. W., Bolot, M., Sarkozy, L., Ebert, V., Saathoff, H., ...
474 Moyer, E. J. (2017, May). Laboratory measurements of $\text{HDO}/\text{H}_2\text{O}$ iso-
475 topic fractionation during ice deposition in simulated cirrus clouds. *Pro-
476 ceedings of the National Academy of Science*, *114*(22), 5612-5617. doi:
477 10.1073/pnas.1618374114
- 478 Mayyasi, M., Bhattacharyya, D., Clarke, J., Catalano, A., Benna, M., Mahaffy,

- 479 P., ... Jakosky, B. (2018, September). Significant Space Weather Im-
 480 pact on the Escape of Hydrogen From Mars. , *45*(17), 8844-8852. doi:
 481 10.1029/2018GL077727
- 482 Mayyasi, M., Clarke, J., Bhattacharyya, D., Chaufray, J. Y., Benna, M., Mahaffy,
 483 P., ... Jakosky, B. (2019, March). Seasonal Variability of Deuterium in the
 484 Upper Atmosphere of Mars. *Journal of Geophysical Research (Space Physics)*,
 485 *124*(3), 2152-2164. doi: 10.1029/2018JA026244
- 486 Moores, J. E., Osinski, G., Whiteway, J. A., & Daerden, F. (2011, March). Strat-
 487 ification of HDO During Cloud Formation on Mars. In *42nd annual lunar and*
 488 *planetary science conference* (p. 1402).
- 489 Moores, J. E., Smith, P. H., & Boynton, W. V. (2011, February). Adsorptive frac-
 490 tionation of HDO on JSC MARS-1 during sublimation with implications for
 491 the regolith of Mars. , *211*(2), 1129-1149. doi: 10.1016/j.icarus.2010.10.020
- 492 Neary, L., Daerden, F., Aoki, S., Whiteway, J., Clancy, R. T., Smith, M., ... Van-
 493 daele, A. C. (2020, April). Explanation for the Increase in High-Altitude
 494 Water on Mars Observed by NOMAD During the 2018 Global Dust Storm. ,
 495 *47*(7), e84354. doi: 10.1029/2019GL084354
- 496 Owen, T., Maillard, J. P., de Bergh, C., & Lutz, B. L. (1988, June). Deuterium
 497 on Mars: The Abundance of HDO and the Value of D/H. *Science*, *240*(4860),
 498 1767-1770. doi: 10.1126/science.240.4860.1767
- 499 Pieris, H., & Jakosky, B. M. (2022, June). Understanding the Evolution of the Mar-
 500 tian Atmosphere through Nitrogen Isotopes. In *Seventh international workshop*
 501 *on the mars atmosphere: Modelling and observations* (p. 3557).
- 502 Shaposhnikov, D. S., Medvedev, A. S., Rodin, A. V., & Hartogh, P. (2019, April).
 503 Seasonal Water “Pump” in the Atmosphere of Mars: Vertical Transport to the
 504 Thermosphere. , *46*(8), 4161-4169. doi: 10.1029/2019GL082839
- 505 Slipski, M., & Jakosky, B. M. (2016). Argon isotopes as tracers for martian atmo-
 506 spheric loss. *Icarus*, *272*, 212–227.
- 507 Stone, S. W., Yelle, R. V., Benna, M., Lo, D. Y., Elrod, M. K., & Mahaffy, P. R.
 508 (2020, November). Hydrogen escape from Mars is driven by seasonal
 509 and dust storm transport of water. *Science*, *370*(6518), 824-831. doi:
 510 10.1126/science.aba5229
- 511 Vandaele, A. C., Korablev, O., Daerden, F., Aoki, S., Thomas, I. R., Altieri,

- 512 F., ... others (2019). Martian dust storm impact on atmospheric H₂
 513 O and D/H observed by ExoMars Trace Gas Orbiter. *Nature*, *568*. doi:
 514 10.1038/s41586-019-1097-3
- 515 Villanueva, G. L., Liuzzi, G., Aoki, S., Stone, S. W., Brines, A., Thomas, I. R., ...
 516 Vandaele, A. C. (2022, June). The Deuterium Isotopic Ratio of Water Re-
 517 leased From the Martian Caps as Measured With TGO/NOMAD. , *49*(12),
 518 e98161. doi: 10.1029/2022GL098161
- 519 Villanueva, G. L., Liuzzi, G., Crismani, M. M. J., Aoki, S., Vandaele, A. C., Daer-
 520 den, F., ... Lopez-Moreno, J. J. (2021, February). Water heavily fractionated
 521 as it ascends on Mars as revealed by ExoMars/NOMAD. *Science Advances*,
 522 *7*(7), eabc8843. doi: 10.1126/sciadv.abc8843
- 523 Villanueva, G. L., Mumma, M. J., Novak, R. E., Käuffl, H. U., Hartogh, P., Encre-
 524 naz, T., ... Smith, M. D. (2015, April). Strong water isotopic anomalies in
 525 the martian atmosphere: Probing current and ancient reservoirs. *Science*,
 526 *348*(6231), 218-221. doi: 10.1126/science.aaa3630
- 527 Vos, E., Aharonson, O., Schörghofer, N., Forget, F., Millour, E., Rossi, L., ...
 528 Montmessin, F. (2022, March). Stratigraphic and Isotopic Evolution of the
 529 Martian Polar Caps From Paleo-Climates Models. *Journal of Geophysical*
 530 *Research (Planets)*, *127*(3), e07115. doi: 10.1029/2021JE007115
- 531 Yung, Y. L., Wen, J.-S., Pinto, J. P., Allen, M., Pierce, K. K., & Paulson, S. (1988,
 532 October). HDO in the Martian atmosphere: Implications for the abundance of
 533 crustal water. , *76*(1), 146-159. doi: 10.1016/0019-1035(88)90147-9
- 534 Zahnle, K., Haberle, R. M., Catling, D. C., & Kasting, J. F. (2008). Photochemical
 535 instability of the ancient Martian atmosphere. *Journal of Geophysical Research*
 536 *E: Planets*, *113*. doi: 10.1029/2008JE003160

Figure 2.

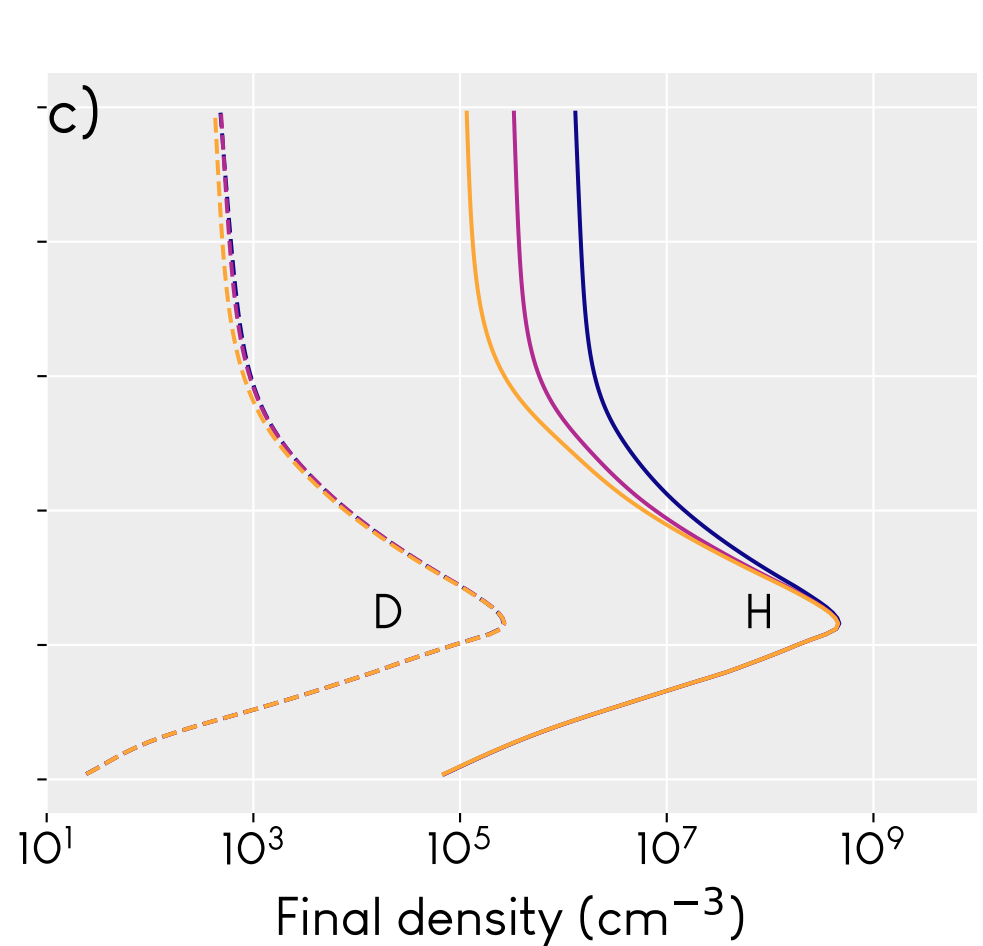
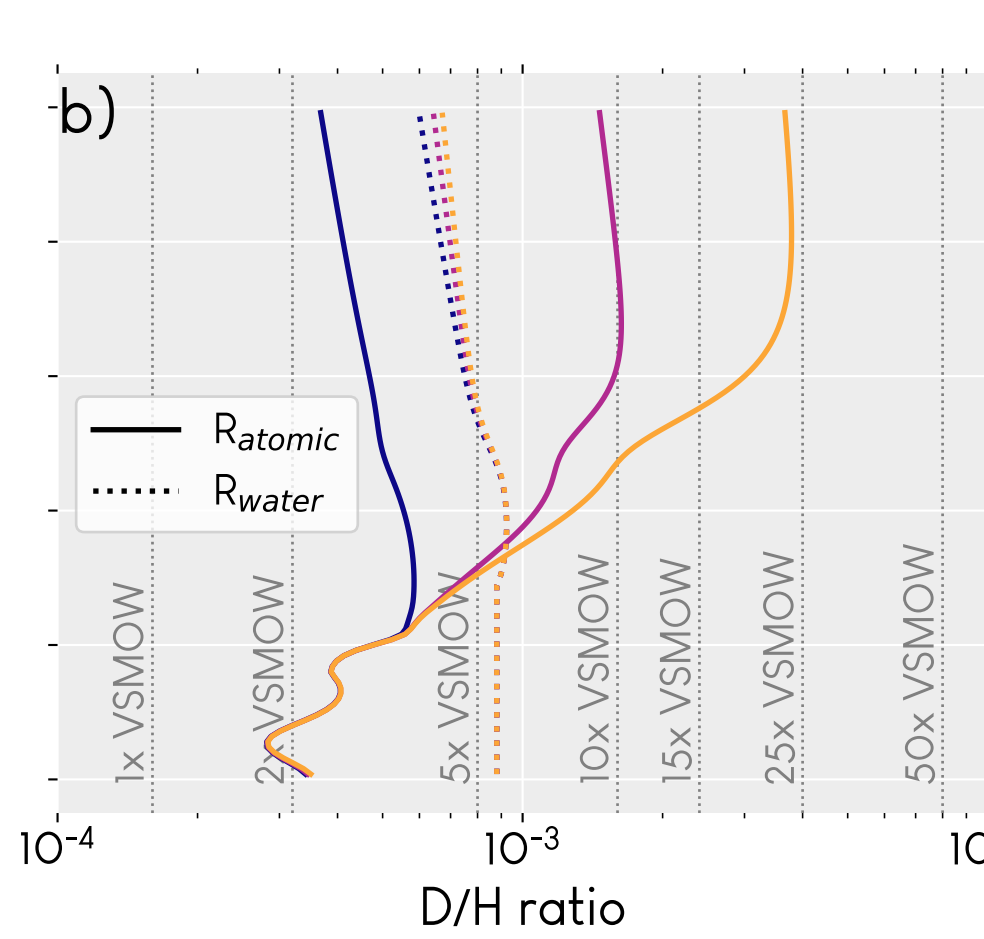
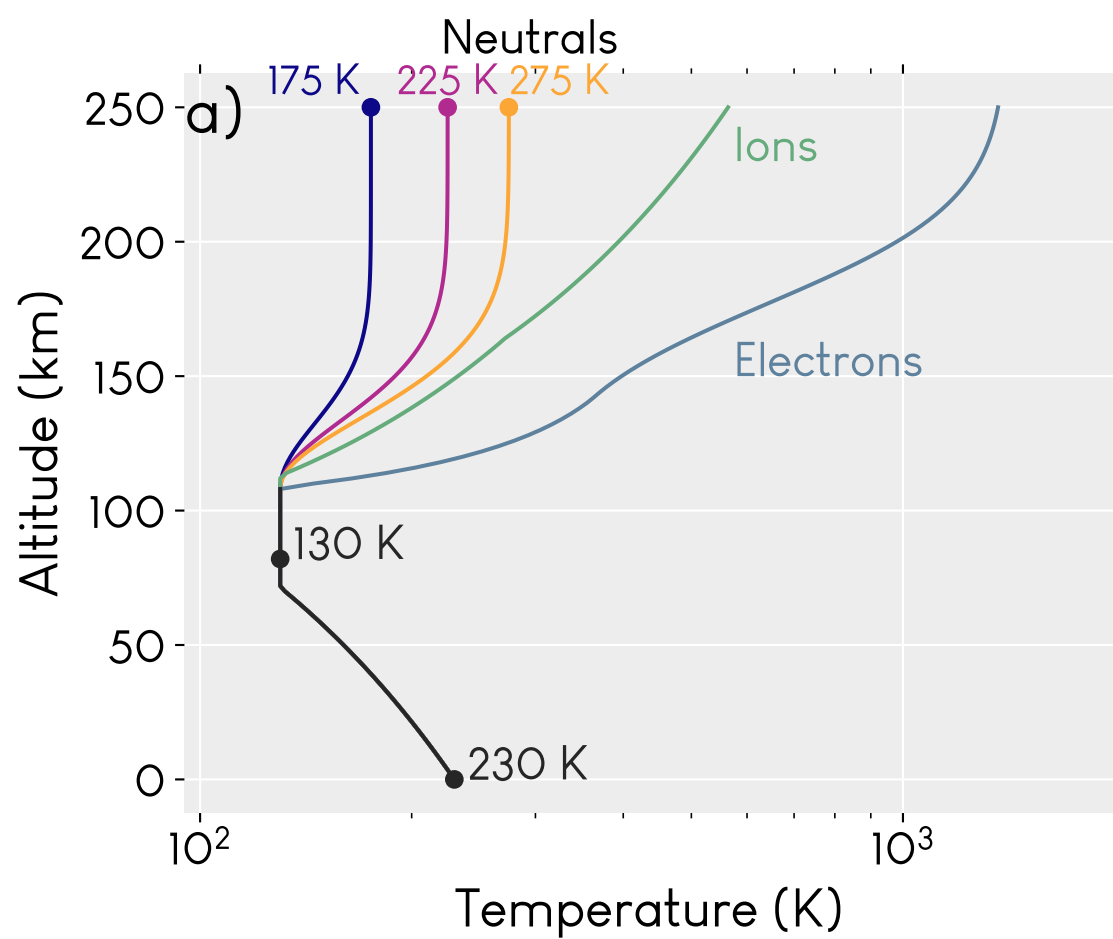


Figure 4.

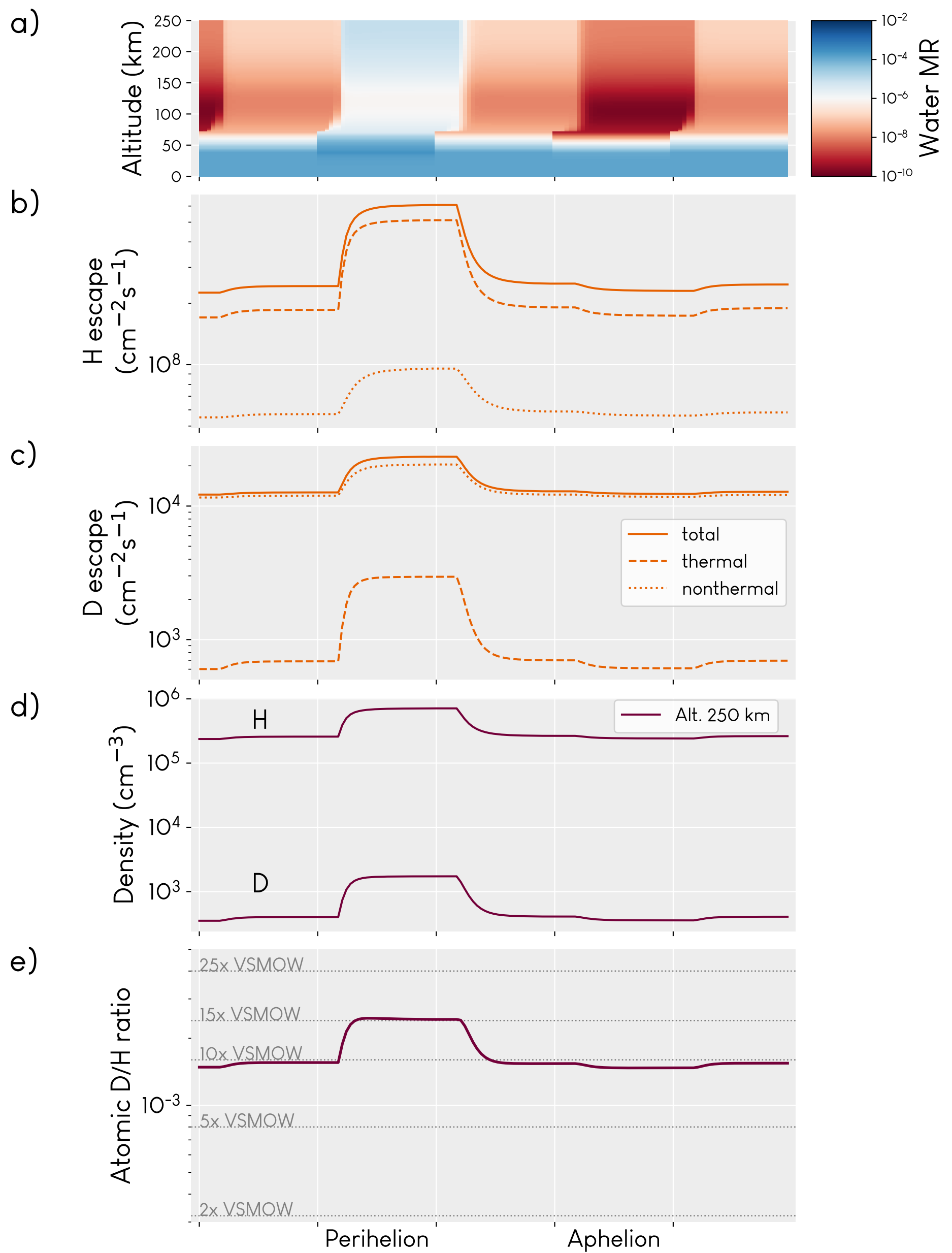


Figure 3.

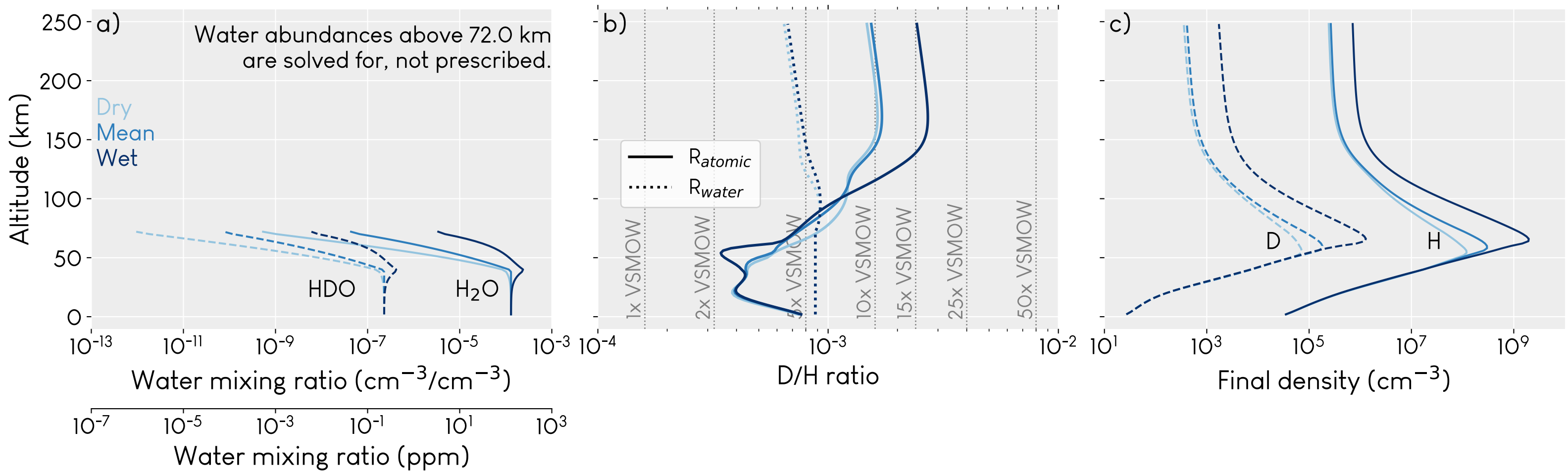


Figure 1.

